Slippery Model for a Semi-Passive Mobile Platform Subject to External Wrenches

S. Shoval
Defence and System Institute
University of South Australia
Mawson Lakes, South Australia, 5095
shraga.shoval@unisa.edu.au

A. Shapiro
Department of Mechanical Engineering
Ben Gurion University
Beer Sheba, Israel

Abstract— **In this paper we describe a slippery model for a mobile robot with multiple independently steered and passively driven wheels, moving on a slippery surface while being subjected to an external wrench. The model determines the vehicle's instantaneous response to the external wrench given the wheels' configuration. The model is verified and tested in a mobile robot that consists of an upper circular body and three identical semi-passive driving mechanisms. Each mechanism consists of a passive wheel that can freely roll, and a rotation actuator along the radial axes. Kinematic analysis provides tools for designing a motion path that steers the robot to the desired location, and determines the singular configurations. Due to the passive roll, there is no longitudinal slippage, and possible lateral slippage is determined by the dynamic model. This slippage can then be verified from kinematic and odometric models.***)**

Keywords—**Passive motion planning, skid steering, slippage**

I. INTRODUCTION

Wheel slippage is one of the dominant features that affect the efficiency, reliability, feasibility and stability of mobile robot motion.. The most common method for autonomous relative position estimate - odometry, is subject to unbounded errors due to slippage [1], and requires an additional positioning system (e.g. Map- Matching, GPS, Beacon-Based Triangulation). This problem becomes critical when no absolute positioning system is available (e.g. space, underground or indoor). Furthermore, additional tasks such as trajectory planning and obstacle avoidance cannot be reliably performed in the presence of uncontrolled slippage. Many researchers deal with robot-surface interaction, particularly on slippery terrains. Bidaud et. al. [2] deal with wheel-soil interaction. Iagnemma et. al. [3] describe terrain estimation and sensing methodology using visual, tactile and vibrational feedback. Ferretti et. al. [4] exploit high resolution encoders to compensate for non linear friction terms. Physics based motion control that involves a model of traction mechanics with the consideration of force distribution among the wheels is discussed in [5]. In this approach the wheel-soil contact angle and the distribution of the load on each wheel are considered, and a control system maximizes traction between the vehicle and the terrain. Yoshida and Hammano [6] investigate the tire-soil traction mechanics as well as the body-suspension-wheel dynamics of a mobile robot.

In this paper we consider a mobile platform with several semi-passive wheels. Each wheel has steering mechanism around the vertical axis (ωi), and no rotation driving mechanism (around the ci axis), as shown in Fig. 1. For simplicity we assume that all mechanical components are perfectly rigid, and all wheels have the same radius. Since the wheels have no rotation mechanisms, we can assume that contacts between the wheels and the ground along the ai axis rolls with no slippage. Accordingly, the velocity of the contact point of each wheel with the ground in the longitudinal direction is equal to zero. We further assume that the platform weight is evenly distributed among all wheels such that the normal forces at all contact points are equal, and that the friction coefficients (both static and dynamic) between the wheels and the ground are the same at all contact points. The latter assumption could be relaxed in two different. First if the robot has only three wheels then the normal forces can be easily computed using the robot's equilibrium equations. In the case where the robot has four or more wheels, the contact forces computation problem is statically indeterminate and could be solved using elasticity and compliance of the wheels' computation.

The mobility of the platform is generated by an external wrench $\Re$. This wrench can comprise of pulling/pushing force(s) extracted by external resources, a propulsion force generated by an on-board generator (e.g. propeller or air-turbine engine) or by a gravitational force (applicable for motion on inclined surfaces).

Given the system shown in Fig. 1, we consider the following problems:

For a given wrench $\Re$ and wheels' configuration $W = (\omega_1, \omega_1, ...\omega_n)^T$, where ω_i is the i^{th} wheel angle with response to the robot's heading direction, what is the instantaneous response of the platform?

For a given a wrench $\Re$, what is the required wheels' configuration W for the platform to follow a given trajectory P?

978-1-4244-1676-9/08 /$25.00 ©2008 IEEE

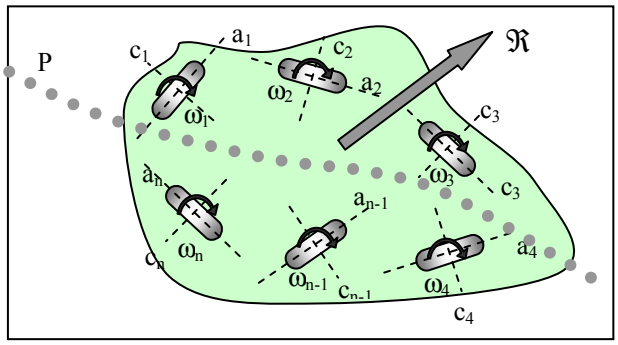

Figure 1. The multi wheeled mobile platform.

II. MODEL FORMULATION

We start by defining the parameters used by the model (Fig. 2):

Nomenclature

d_b : Position of the center of the platform

θ_b : Platform orientation

p_i : Position of the center of the i^{th} wheel

ω_i : Rotation of the i^{th} wheel along the normal to the platform, with respect to the body x axis.

$\hat{r}_i$: Unit vector from the center of the platform to the contact of the i^{th} wheel with the ground, given in body frame.

l_i : The distance between the origin of the body frame and the contact point of the i^{th} wheel with the ground

$\hat{c}_i$: Unit vector in the lateral direction of the i^{th} wheel, given in body frame.

ϕ_i : Rolling angle of the i^{th} wheel.

The position of the i^{th} wheel is determined by

$$p_i = d_b + R_b l_i \hat{r}_i. \tag{1}$$

Assuming $\hat{r}_i$ is held constant the velocity is given by:

$$\dot{p}_i = \dot{d}_b - \dot{\theta}_b J R_b l_i \hat{r}_i + R_b \dot{l}_i \hat{r}_i. \tag{2}$$

Where $J = \begin{bmatrix} 0 & 1 \\ -1 & 0 \end{bmatrix}$ and R_b is the rotation matrix of the body frame with respect to the world frame.

If there is no lateral slippage then we can write

$$c_i^T \dot{p}_i = 0 \quad \text{for i=1,2,..n} \tag{3}$$

where n is the number of wheels in the system.

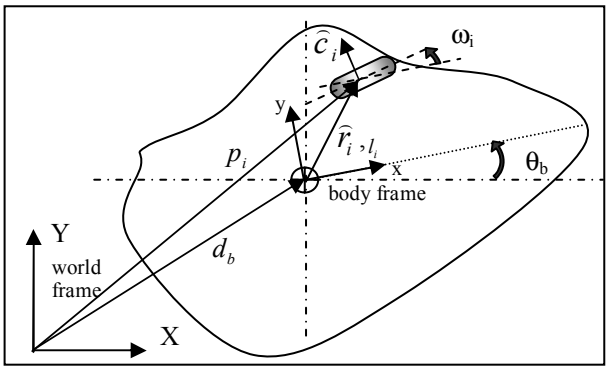

Figure 2. Schematic diagram of the i^{th} wheel.

Next, we define the *K(q)* matrix:

$$K(q) = \begin{pmatrix} c_1^T & l_1 c_1^T J R_b \hat{r}_1 \\ c_2^T & l_2 c_2^T J R_b \hat{r}_2 \\ ..... & ..... \\ c_{n-1}^T & l_{n-1} c_{n-1}^T J R_b \hat{r}_{n-1} \\ c_n^T & l_n c_n^T J R_n \hat{r}_n \end{pmatrix} \in \Re^{n\times 3} \tag{4}$$

where $q = (x_b, y_b, \theta_b, \omega_1, \omega_2, ...\omega_n)^T \in \Re^{n+3}$ is the configuration space of the platform.

We also define the V(q) matrix to be:

$$V(q) = -diag(c_1^T R_b l_1 \hat{r}_1, c_2^T R_b \hat{r}_2, ...c_n^T R_b l_n \hat{r}_n) \in \Re^{n\times n} \tag{5}$$

In general the no lateral slippage condition (3) can be expressed as:

$$K(q)\begin{pmatrix} \dot{d}_b \\ \dot{\theta}_b \end{pmatrix} = V(q)\begin{pmatrix} \dot{l}_1 \\ \vdots \\ \dot{l}_n \end{pmatrix} \tag{6}$$

In case the robot has only three wheels, the robot's *Jacobean matrix* can be defined as

$$J(q) = K^{-1}(q)V(q) \in \Re^{3\times 3} \tag{7}$$

In this particular case the central body's velocities can be computed explicitly based on (6),

$$\begin{pmatrix} \dot{d}_b \\ \dot{\theta}_b \end{pmatrix} = J(q)\begin{pmatrix} \dot{l}_1 \\ \dot{l}_2 \\ \dot{l}_3 \end{pmatrix} \tag{8}$$

Let us define lines along the axes of the three robot's wheels as follows:

$$m_i = d_b + l_i R_b \hat{r}_i + t_i \hat{c}_i \quad \text{for } i=1,2,..n \tag{9}$$

where t_i is a length parameter along m_i line (Fig. 3). For any random combination *(a,b,c)* of three wheels we construct the K*(q) matrix:

$$K^*(q^*) = \begin{pmatrix} c_a^T & l_a c_a^T J R_b \hat{r}_a \\ c_b^T & l_b c_b^T J R_b \hat{r}_b \\ c_c^T & l_c c_c^T J R_b \hat{r}_c \end{pmatrix} \in \Re^{3\times 3} \qquad (10)$$

where $q^* = (a,b,c)$ is a triplet which is a subset of the *n* wheels set for a given wheels' configuration.

Theorem 1: Matrix K*(q*) is of full rank if, and only if, the three lines m_a,m_b, and m_c do not intersect at a single point or are not parallel to each other (in this case the intersection point is in the infinity).

The proof of this theorem is based on the solution of the three lines (Eq. 9) for t_i (deterring the values of t_a, t_b, and t_c) and comparing it to the singularity conditions of K*(q*). The detailed proof of the theorem is beyond the scope of this paper.

Theorem 1 provides an effective formulation for determining singularity configurations. These configurations occur when the lateral direction of all wheels are either parallel to each other or intersect at a single point. The following Corollary asserts a sufficient and effective condition for the matrix K(q) to be of full rank.

Corollary 1: If the matrix $K^*(1,2,x)$ is of full rank for $x=3$ *to n*, then the matrix $K(q)$ is of full rank.

Proof: In order for K(q) to be of full rank lines m_i for i=1,..,n must not intersect at a single point or be mutually parallel. Therefore it is sufficient to check whether all lines m_i for i=3,..,n pass through the intersection point of m_1 and m_2. Moreover, in case of m_1 parallel to m_2 it is also sufficient to check that all other lines are parallel to these lines.

Finally, we define the Non-Singularity Index (NSI) which is the number of triplets q* that construct a non singular matrix K*(q*) for a given wheels configuration.

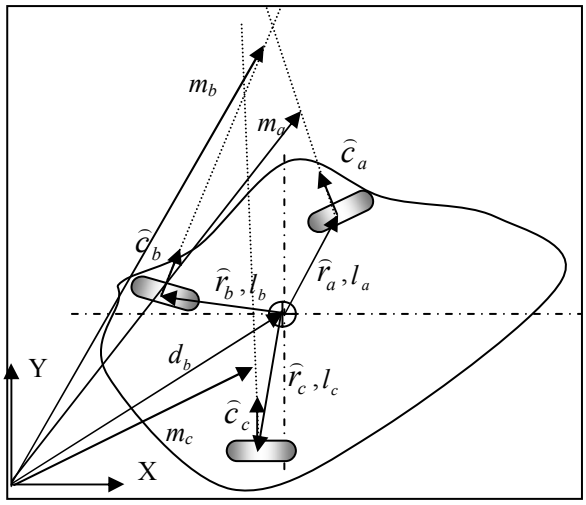

Figure 3. Schematic a subset consists of three wheels

III. MODEL SOLUTION

In the previous section we discussed the conditions for singularity of the wheels' configuration which determines if the lateral directions of all the wheels are mutually parallel or intersect at a single point. Returning to the original scenario shown in Fig. 1, we can now determine the instantaneous response of the platform while a given wrench $\Re$ is applied to the robot. We classify two possible wheels' configuration types according to NSI:

NSI>0: In this configuration there is at least one subset of q* that is not singular. As a result, the platform is considered to be at a ***limited force closure*** configuration. In this configuration the wheels are capable of balancing the external wrench $\Re$ by applying a reaction forces f_i^c at the contact points (p_i) of the wheels with the ground such that

$$\Re + \Theta(p_1, p_2, ..p_n, f_1^c, f_2^c, ...f_n^c) = 0 \qquad (11)$$

where Θ maps each reaction force to the resulting wrench on the platform frame. Note that (11) is the six dimensional equilibrium equations. The limit on the force closure configuration is due to the limits on the lateral static friction between the wheels and the surface. It is important to mention here that (11) consists of the following: Three equations which state that the sum of the forces is zero, and three equations which state that the sum of the torques is zero. For the case of three wheeled robot equation, we have six unknowns: normal force and lateral friction force for each wheel. Therefore for a three wheeled robot we can easily compute the contact forces using six equilibrium equations with six unknowns. However for robot with a higher number of wheels we need to exploit elasticity and compliance in order to solve the statically indeterminate problem.

NSI=0: In this configuration all subsets of q* are singular, so lateral directions of all the wheels intersect at a single point, as shown in Fig. 4. We call this configuration ***limited rotational configuration***. For a given external wrench $\Re$ and friction constraints, the platform can rotate around this intersection point. The following sections discuss the two types of configurations with more details.

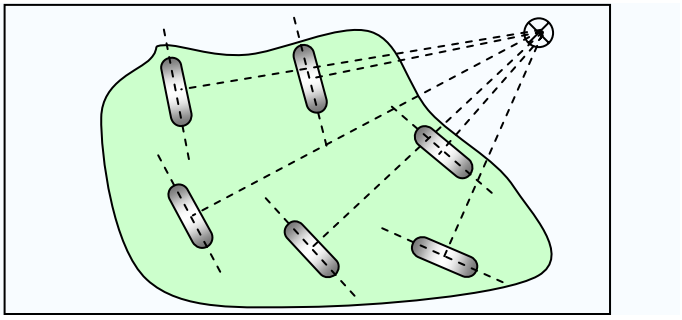

Figure 4. NSI=0 – all lateral directions intersect at a single point

IV. LIMITED FORCE CLOSURE CONFIGURATION

As discussed in the previous section, the wheels are capable of balancing the external wrench $\Re$ in the limited force closure configuration according to Eq.11, subject to the friction constraints, given by

$$f_i^c \le \mu_s N_i \quad for \;\; i=1 \; to \; n \tag{12}$$

where μ_s is the static friction coefficient at the contact of the i^{th} wheel and the ground, and N_i is the normal force applied by the i^{th} wheel.

If all lateral forces are within the friction constraints, the platform is at force closure configuration and there is no slippage. In case NSI>0 the platform will remain static. If the lateral force on one wheel reaches the friction constraint, the platform may remain in force closure, but now Eq. (11) is applied on *n-1* wheels with two wrenches: the original external wrench $\Re$, and an additional wrench $\Re^*$ applied by the friction force.

$$\Re^* = \begin{pmatrix} \mu N_i \hat{c}_i \\ \mu N_i l_i \hat{c}_i \times \hat{r}_i \end{pmatrix} \tag{13}$$

Equation (9) is now updated to

$$\Re + \Re^* + \Theta(p_1, p_2, .. p_{n-1}, f_1^c, f_2^c, ... f_{n-1}^c) = 0 \tag{14}$$

The process can now be repeated for the *n-1* wheels. If two or more reaction forces remain within the friction constraints, and if their respective $K^*(q^*)$ is of full rank, then the platform is at force closure. If only one reaction force remains within the friction constraints, the platform will start rotating around the intersection point of their respective lines m_i, or about the contact point of the remaining wheel. At this stage the other wheels will start a combined rolling and lateral slippage motion. When the last wheel reaches the friction constraint, the platform moves according the external wrench, the dynamic friction forces, and the dynamics of the robot. To verify our model we developed a three wheeled prototype platform shown in Figure 5 and 6.

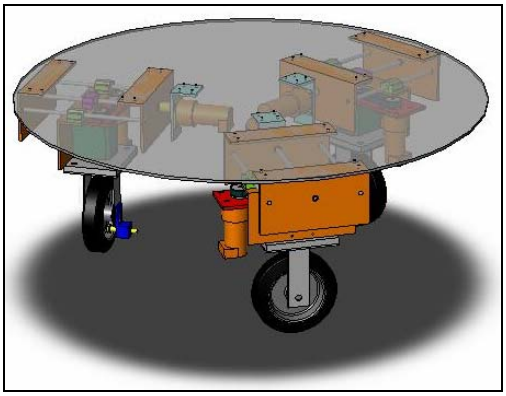

Figure 5. Design model of our three wheeled robot.

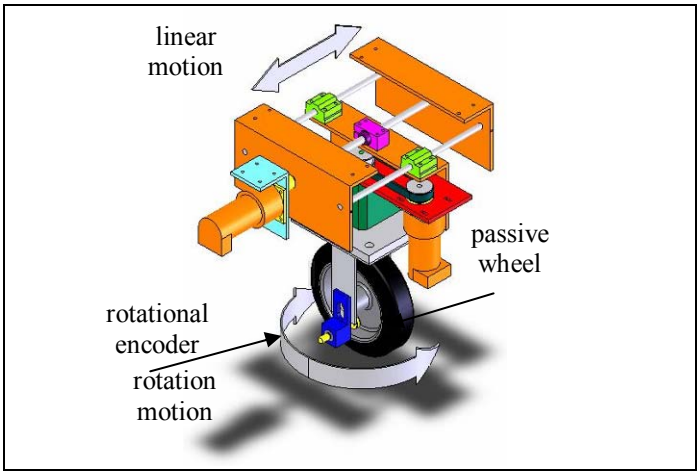

Figure 6. Design model of the wheel mechanism

Figure 7(a) shows a snapshot from our simulator that describes a specific wheel configuration of the platform. In this configuration the wheels are directed at 30°, 0°, and 90°. This configuration is a ***limited force closure***, as the lateral wheels' directions do not intersect at a single point and are not mutually parallel. The external wrench is generated by a force applied on the platform in the X+ direction. Figure 7b shows the lateral reaction forces as a function of increasing external force. The limit of the static friction forces (combined with a constant normal force) for the given experiment is 500N. In this case wheel #3 is the first to reach the friction constraint when the magnitude of the external forces is 667N. The reaction forces on wheels #1 and #2 are 333N and 289N respectively. If the external force continues to increase, the reaction force on wheel #3 remains at 500N and the other reactions forces increase as shown in Fig. 7c. In this case the robot will rotate around the intersection point of m_1 and m_2. After further increase of the external force to 752N the reaction force on wheel #1 reaches the friction constraint. Further increase in the external force eventually cause wheel #2 to also reach its static friction constraint, and start lateral slippage.

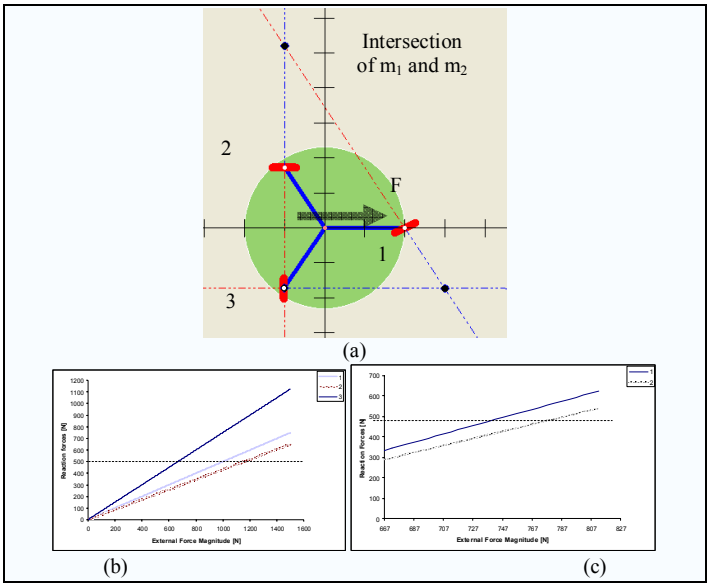

Figure 7. Wheels' configuration (a) and reaction forces (b and c)

V. LIMITD ROTATIONAL CONFIGURATION

We now consider the case of NSI=0, when the lateral directions of all wheels intersect at a single point – O (Fig. 8). We define the radius of curvature R as the distance between the intersection point O and the center of mass of the body C. We then divide the force F to its tangential (F_t) and radial (F_r) components. The tangential force F_t causes the platform to rotate around O, while the radial force F_r causes lateral reaction forces at the wheels' contacts with the ground. These reaction forces are also a result of the centripetal acceleration due to the rotational movement. As long as the lateral reaction forces are within the friction constraints, the platform continues its rotational motion. When the lateral reaction forces reach friction constraints, lateral slippage occurs, combined with the rotational motion. The robot starts a circular motion around O at an initial speed V_i, and, when it reaches critical speed V_c, it starts a combined rolling circular motion and lateral slippage motion. The critical speed can be determined by

$$V_c = \sqrt{\frac{R(F_r + \sum_{i=1}^{n} (F_i^f \bullet \hat{R})}{m}} \tag{15}$$

where F_i^f is the lateral friction force applied on wheel i, and $\hat{R}$ is a unit vector in the radial direction. This combined rolling and lateral slippage motion results in a slip angle (the angle between a wheel's actual direction of travel and the longitudinal rolling direction). The slip angle is defined by the angle of the vector sum of a wheel's longitudinal velocity $V_{longitudinal}$ and the lateral velocity $V_{latweral}$

$$\alpha = \left(\frac{V_{lateral}}{|V_{longitudinal}|} \right) \tag{16}$$

This slip angle results in a force, perpendicular to the wheel's direction of travel known as the cornering force. This cornering force increases approximately linearly for the first few degrees of slip angle, and then increases non-linearly to a maximum before beginning to decrease. The actual cornering force is a function of the wheel's material and shape, terrain condition and the normal force at the contact point. The ratio between the slip angles of the front and back wheels determines the platform's behavior. If the ratio is larger than 1, then the platform is understeered. If the ratio is less than 1 the platform is oversteered.

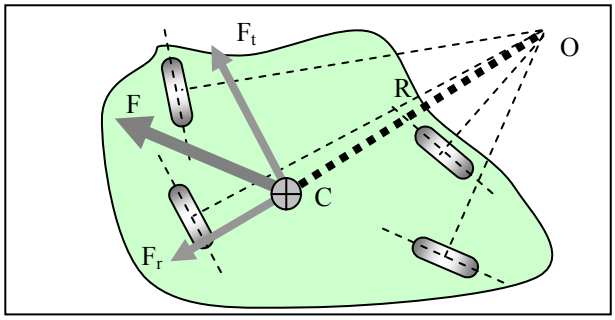

Figure 8. Limited Rotational Configuration

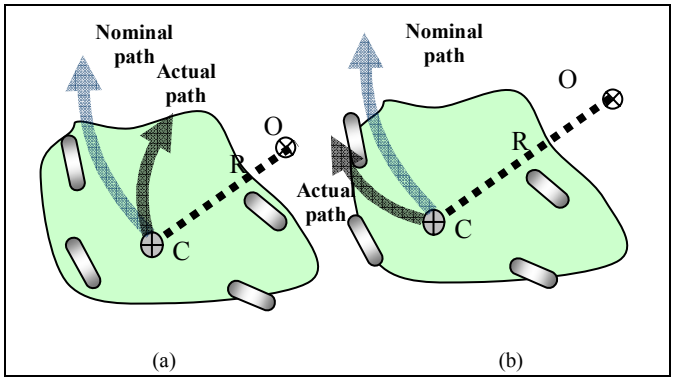

Figure 9. The effect of oversteer (a) and (b) understeer on the platform

During understeered motion the platform moves at a larger radius than the one determined by the distance between the intersection of all lateral wheels' directions and the platform's center. In oversteered motion, on the other hand, the rear wheels slide out toward the outside of the curve, and bring the platform into a spin. Figure 9 shows the effect of oversteered (Fig. 9a) and understeered (Fig. 9b) motion on the platform shown in Fig. 8.

VI. EXPERIMENTAL RESULTS

To verify our slippage models we performed several experiments using our Glider Prototype Robot (Fig. 10). In the first experiment, the robot was traveling downhill on a flat surface with wheels #1 and #3 in front and #2 at the back (Fig 11a). At the beginning of the experiment, all wheels point to the front ($\theta_1 = \theta_3 = 0^0$). During the 20 second experiment, wheels #1 and #3 symmetrically and linearly rotate inwards, while wheel #2 is subjected to random rotation in the range of $\pm 5^o$, as shown in Fig. 11(b). As a result of the changing rotation angle of wheels #1 and #3, lateral slippage occurs affecting the roll speed of each wheel, as shown in Fig. 11(c), until the robot stops. As expected, lateral slippage increases as the rotation angle increases, similar to the models shown in Shiller and Gwo [8]. These results are consistent with our previously developed kinematic and odometric models [9].

Figure 10. The Glider Prototype Robot

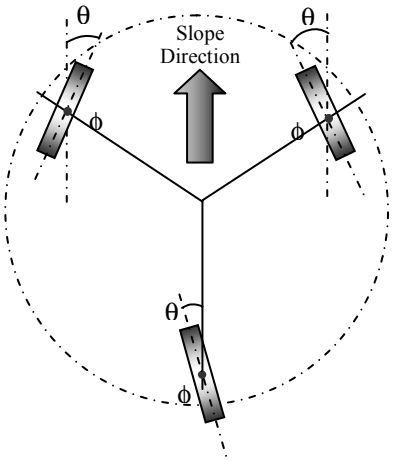

11(a) – Configuration of the robot during the experiment

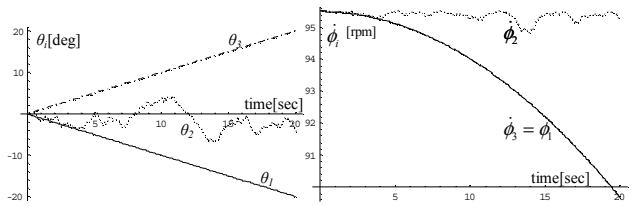

11(b) - Changes in rotation angle 11(c)- Changes in rolling speeds

Figure 11. Experimental results of linear motion

In the next experiment the robot is at a singular configuration such that the lines l_i's intersect at a single point. In this case the robot is constrained to move along an arc shaped path. The center of the arc is in the intersection point of the l_1,l_2 and l_3 lines. Since the robot is an Euler-Lagrange system and there is friction in the wheels' bearings, then the system is passive and governed by gravitational potential energy. According to Koditschek [10] the configuration in which the system's potential energy is minimal is an asymptotical stable equilibrium point of the system. According to this observation, we find the radius and center of curvatures at each point of the desired motion path. Then we continuously set the l_i's intersection point at the center of curvature of the desired path by changing the robot's configuration. This way, the robot passively glides along the desired path (Fig. 12).

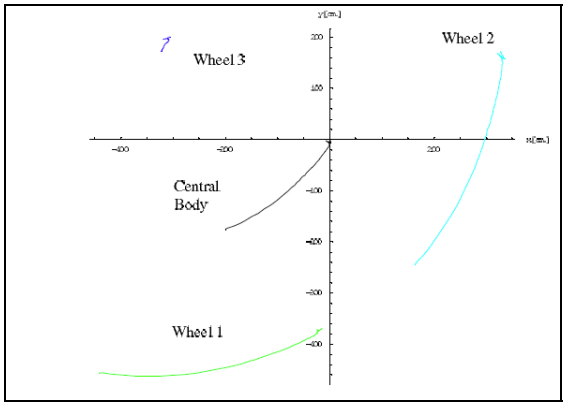

Figure 12. Experimental results of linear motion

VII. CONCLUSIONS

In this paper we present a model for motion of a semi-passive mobile robot subject to external wrench. The robot consists of a base platform and multiple semi passive wheels. Each wheel can actively rotate around the normal to the central base and passively roll along the longitudinal direction. The model analyzes the reaction forces and possible lateral slippage of the wheels. Based on this analysis the model determines the boundaries of the external wrench that maintain the robot in a force-closure configuration. The model also determines the singular configurations in which the robot performs linear and circular motion, as well as the limitations for non-slippage motion. Field experiments, using a three wheeled platform robot have been conducted to verify our model. These experiments can be found in our website: http://www.ariel.ac.il/iem/pf/shoval/index_files/Shraga%20Shoval,%20Publications.htm.

REFERENCES

[1] J. Borenstein and L. Feng, "Gyrodometry: A new method for combining data from gyros and odometry in mobile robots," *IEEE Int. Conf. on Robotics and Automation*, Minneapolis, Minnesota, April 1996, pp. 423–428.

[2] Bidaud, R. Chatila, G. Andrade-Barroso, and F. B. Amar, "Modeling robot-soil interaction for planetary rover motion control," *IEEE/RSJ Int. Conf. on Intelligent Robots and Systems*, Victoria B.C., Canada, October 1998, pp. 576–581.

[3] K. Iagnemma and S. Dubowsky, "Vehicle wheel-ground contact angle estimation: with application to mobile robot traction control," *7th Int. Symposium on Advances in Robot Kinematics*, Piran-Portoroz, Slovenia, June 2000.

[4] G. Ferretti, G. Magnani, G. Martucci, P. Rocco, and V. Stampacchia, "Friction model validation in sliding and presliding regimes with high resolution encoders," *Experimental Robotics VIII B. Siciliano and P. Dario Eds.* Heidelberg: STAR Springer, 2002, pp. 328–337.

[5] S. Dubowsky and K. Iagnemma, "Mobile robot rough-terrain control (rtc) for planetary exploration," *Proceedings of ASME DETC/CIE: 26th Biennial Mechanisms and Robotics Conference*, Baltimore, Maryland, September 2000.

[6] K. Yoshida and H. Hamano, "Motion dynamics of a rover with slip-based traction model," *IEEE Int. Conf. on Robotics and Automation*, Washington D.C., May 2002, pp. 3155–3160. New Orleans, LA, April 2004, pp. 3944–3949.

[7] E. Rimon and J.W. Burdick, "Mobility of Bodies in Contact—Part I: A 2nd-OrderMobility Index for Multiple-Finger Grasps", *IEEE Transaction on robotics and Automation,* Vol. 14, No. 4, 1998, pp. 696-708.

[8] Shiller, Z., Gwo R.Y., "Dynamic Motion Planning of Autonomous Vehicles," *IEEE Journal of Robotics and Automation*, Vol. 7, No. 2, April 1991, pp. 241-249.

[9] Shapiro A., and Shoval S., "Design and Locomotion of a Semi-passive Mobile Platform", *Springer Tracts in Advanced Robotics*, Volume 25 / 2006, pp. 319 – 330.

[10] D. E. Koditschek, "The application of total energy as a lyapunov function for mechanical control systems," *J. Marsden, Krishnaprasad, and J. Simo, editors, Control Theory and Multibody Systems, AMS Series in Contemporary Mathematics*, Vol. 97, pp. 131–158, 1989.